Small-Molecule Inhibitors of the Programmed Cell Death-1/Programmed Death-Ligand 1 (PD-1/PD-L1) Interaction via Transiently Induced Protein States and Dimerization of PD-L1

Guzik, Katarzyna; Zak, Krzysztof M.; Grudnik, Przemyslaw; Magiera, Katarzyna; Musielak, Bogdan; Törner, Ricarda; Skalniak, Lukasz; Dömling, Alexander; Dubin, Grzegorz; Holak, Tad A.

Published in:
Journal of Medicinal Chemistry

DOI:
10.1021/acs.jmedchem.7b00293

Publication date:
2017

Journal of Medicinal Chemistry

Article

pubs.acs.org/jmc

Small-Molecule Inhibitors of the Programmed Cell Death-1/Programmed Death-Ligand 1 (PD-1/PD-L1) Interaction via Transiently Induced Protein States and Dimerization of PD-L1

Katarzyna Guzik,[†] Krzysztof M. Zak,[‡,§] Przemyslaw Grudnik,[‡,§] Katarzyna Magiera,[†,§] Bogdan Musielak,[†] Ricarda Törner,[†] Lukasz Skalniak,[†] Alexander Dömling,[∥] Grzegorz Dubin,[‡,§] and Tad A. Holak*[,†,§]

[†]Department of Organic Chemistry, Faculty of Chemistry, Jagiellonian University, Ingardena 3, 30-060 Krakow, Poland

[‡]Faculty of Biochemistry, Biophysics and Biotechnology, Jagiellonian University, Gronostajowa 7, 30-387 Krakow, Poland

[§]Malopolska Centre of Biotechnology, Jagiellonian University, Gronostajowa 7a, 30-387 Krakow, Poland

[∥]Department for Drug Design, University of Groningen, A. Deusinglaan 9, AV 9713 Groningen, The Netherlands

Supporting Information

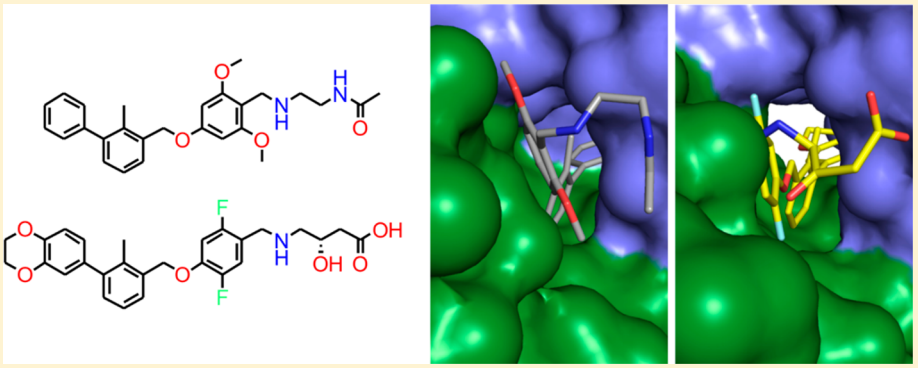

ABSTRACT: Blockade of the PD-1/PD-L1 immune checkpoint pathway with monoclonal antibodies has provided significant advances in cancer treatment. The antibody-based immunotherapies carry a number of disadvantages such as the high cost of the antibodies, their limited half-life, and immunogenicity. Development of small-molecule PD-1/PD-L1 inhibitors that could overcome these drawbacks is slow because of the incomplete structural information for this pathway. The first chemical PD-1/PD-L1 inhibitors have been recently disclosed by Bristol-Myers Squibb. Here we present NMR and X-ray characterization for the two classes of these inhibitors. The X-ray structures of the PD-L1/inhibitor complexes reveal one inhibitor molecule located at the center of the PD-L1 homodimer, filling a deep hydrophobic channel-like pocket between two PD-L1 molecules. Derivatives of (2-methyl-3-biphenylyl)methanol exhibit the structures capped on one side of the channel, whereas the compounds based on [3-(2,3-dihydro-1,4-benzodioxin-6-yl)-2-methylphenyl]methanol induce an enlarged interaction interface that results in the open "face-back" tunnel through the PD-L1 dimer.

INTRODUCTION

Immune checkpoint blocking (ICB) antibodies that target cytotoxic-T-lymphocyte-associated protein 4 (CTLA4) or programmed death protein 1 (PD-1)/programmed cell death ligand 1 (PD-L1) constitute direct clinical proof that cancer can be treated through the modulation of immunity. ICB-based immunotherapy elicits durable antitumor responses and long-term remissions in a subset of patients with a broad spectrum of cancers.[1−6]

Until now, the anti-CTLA4 antibody (ipilimumab) and three therapeutic antibodies targeting both PD-1 and PD-L1 immune checkpoint proteins (nivolumab, pembrolizumab, and atezolizumab) have gained the U.S. Food and Drug Administration (FDA) acceptance, and several others are currently undergoing clinical trials.[4−11] The antibodies approved are directed against metastatic melanoma, non-small-cell lung cancer (NSCLC) and renal cell carcinoma. In addition encouraging preclinical and clinical results showed that anti-PD-1 and anti-CTLA-4 antibodies combined with each other or with other therapeutics can significantly enhance efficacy and percentage of responders.[4−11]

Development of small molecules that interfere with the PD-1/PD-L1 pathway is lagging in comparison to the development of the antibodies. This partially can be associated with incomplete structural information about these proteins. The structures of the murine PD-1 in complexes with the human PD-L1 (hPD-L1) and murine PD-L2 have established the molecular principles of their interaction.[12,13] Structures of human apo-PD-1 (PDB 3RRQ) and apo-PD-L1 (3BIS, 3FN3,

Received: April 12, 2017
Published: June 14, 2017

DOI: 10.1021/acs.jmedchem.7b00293
J. Med. Chem. 2017, 60, 5857−5867

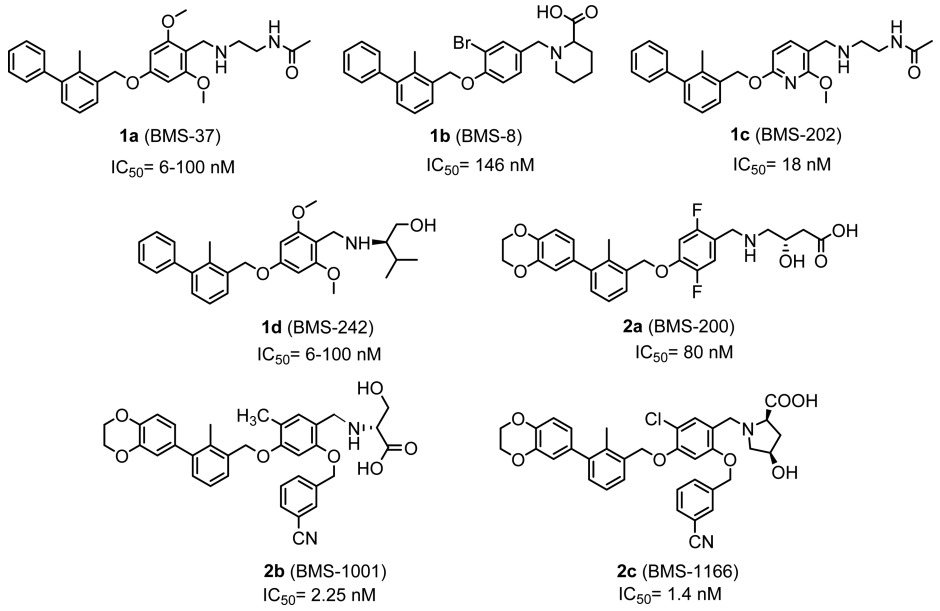

Figure 1. Structures of the synthesized compounds with their IC_{50} values established by the HTRF binding assay. Names of the compounds reported in the patents[18,19] are shown in parentheses.

Table 1. General Pathway for the Synthesis of (2-Methyl-3-biphenylyl)methanol Derivatives 1a, 1b, 1c and 1d[a]

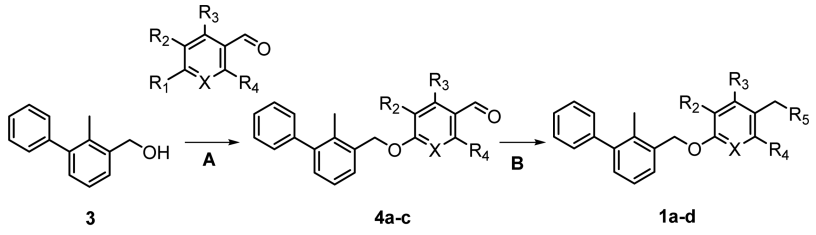

Compound	R_2	R_3	R_4	X	R_5
4a	-H	$-OCH_3$	$-OCH_3$	C	-
4b	-Br	-H	-H	C	-
4c	-H	-H	$-OCH_3$	N	-
1a	-H	$-OCH_3$	$-OCH_3$	C	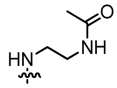
1b	-Br	-H	-H	C	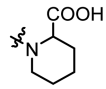
1c	-H	-H	$-OCH_3$	N	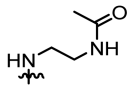
1d	-H	$-OCH_3$	$-OCH_3$	C	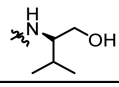

[a](A) PPh_3, DIAD or $Pd(OAc)_2$ or *tert*-butyl XPhos if R_1 is OH or Cl, respectively; (B) amine component R_5, $NaBH_3CN$, AcOH, DMF.

4Z18, 5C3T) have also been determined. The structure of the fully human PD-1/PD-L1 complex, recently solved by us, indicated that the PD-L1 ligand binding to the human PD-1 (hPD-1) is associated with significant plasticity within the receptor.[14]

Small-molecule ICBs of the PD-1/PD-L1 interaction would offer complementary and potentially synergistic therapeutics in comparison to the mAbs. A few series of small molecules, macrocyclic peptides, peptides, and peptidomimetics targeting the PD-1/PD-L1 interaction were reported.[15−17] Bristol-Myers-Squibb (BMS) disclosed recently the first nonpeptidic small-molecule inhibitors against the PD-1/PD-L1 pathway that showed the activity in a homogeneous time-resolved fluorescence (HTRF) binding assay; however no further data supporting their activity were provided.[18,19] Recently, we reported the first cocrystal structures of hPD-L1 complexed with small molecular weight inhibitors disclosed in the BMS patent (PDB codes 5J89, 5J8O).[20] The X-ray and biochemical data revealed that protein dimerization is induced upon ligand binding. Here, we present structural characterization of two

DOI: 10.1021/acs.jmedchem.7b00293
J. Med. Chem. 2017, 60, 5857−5867

Table 2. General Pathway for the Synthesis of [3-(2,3-Dihydro-1,4-benzodioxin-6-yl)-2-methylphenyl]methanol Derivatives 2a, 2b, and 2c[a]

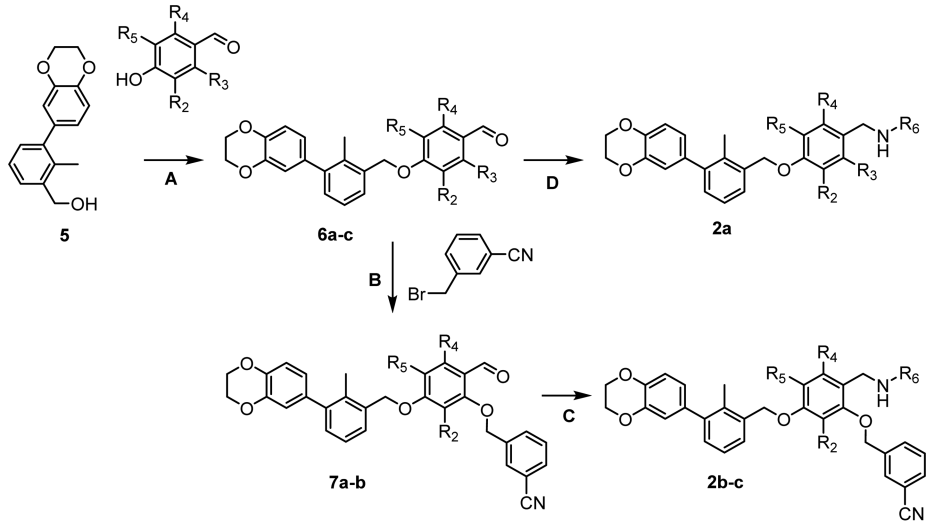

Compound	R_2	R_3	R_4	R_5	R_6
6a	-F	-H	-F	-H	-
6b	-H	-OH	-H	$-CH_3$	-
6c	-H	-OH	-H	-Cl	-
7a	-H	-	-H	$-CH_3$	-
7b	-H	-	-H	-Cl	-
2a	-F	-H	-F	-H	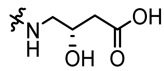
2b	-H	-	-H	$-CH_3$	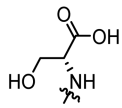
2c	-H	-	-H	-Cl	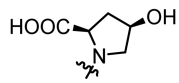

[a](A) PPh_3, DIAD, 0 °C to rt, 20 h, anh THF; (B) Cs_2CO_3, DMF, rt, overnight; (C, D) amine component R_6, $NaBH_3CN$, AcOH, DMF, 80 °C (3 h), then rt (overnight).

further groups of the BMS compounds: the derivatives based on the scaffold of (2-methyl-3-biphenylyl)methanol (compounds **1**, Figure 1) and those based on the [3-(2,3-dihydro-1,4-benzodioxin-6-yl)-2-methylphenyl]methanol (compounds **2**, Figure 1).[18,19] Both bind to the dimeric PD-L1. Recently, we reported the first cocrystal structures of PD-L1 complexed with small molecular weight inhibitors (PDB codes 5J89, 5J8O) disclosed in BMS patent (Zak et al., 2016). Furthermore, our biochemical data revealed that protein dimerization is induced upon ligand binding. Here, we present the two novel crystal structures of disclosed compounds (**1a**, **2a**) both bound to dimeric PD-L1. Our structural studies revealed that upon complex formation one of investigated compound (**2a**) induces conformational changes in the PD-L1 binding site. Thus, this flexible binding site opens new possibilities for the design of improved PD-1/PD-L1 pathway antagonists.

RESULTS

Synthesis of the PD-1/PD-L1 Inhibitors 1a−d and 2a−c. Figure 1 shows the two groups of representative BMS compounds synthesized by us. The first group comprises derivatives of (2-methyl-3-biphenylyl)methanol, **1a−d**. The second one incorporates replacing the distal phenyl ring of **1** by the 2,3-dihydrobenzo[*b*][1,4]dioxinyl moiety, compounds **2a−c**. Both groups of the compounds have their IC_{50} of binding to hPD-L1 in the range of 1.4−146 nM.[18−20]

We also partitioned the large **1** and **2** ligands and screened the resulting fragments for binding to PD-L1 and PD-1. The

DOI: 10.1021/acs.jmedchem.7b00293
J. Med. Chem. 2017, 60, 5857−5867

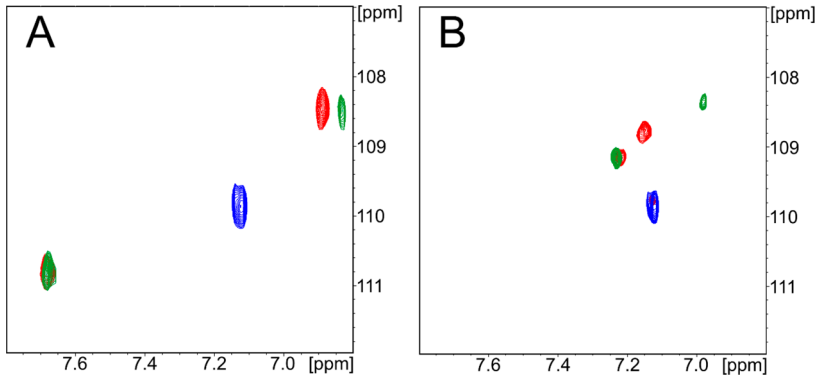

Figure 2. $^{1}H-^{15}N$ 2D HMQC NMR spectra of the [^{15}N-Val]-hPD-L1. (A) apo-PD-L1 (blue) and the compound **1**-induced changes in the NMR chemical shifts, **1a** (red) and **1c** (green). (B) apo-PD-L1 (blue) and the **2**-induced changes in NMR spectra, **2a** (red) and **2b** (green).

fragments that were synthesized contain the biphenyl central scaffold of the BMS compounds (Supporting Information Tables S1 and S2).

Synthesis of the (2-Methyl-3-biphenylyl)methanol Derivatives (1a−d) and Others between (3-Bromo-2-methylphenyl)methanol and Phenylboronic Acid. A large number of biphenyl fragments were obtained using the same methodology (Supporting Information Tables S1 and S2). The Mistunobu reaction or the palladium-mediated Buchwald−Hartwig cross coupling between compound **3** and an appropriately substituted aldehyde provided aldehydes **4a−c**.[21,22] In the last step the $NaBH_3CN$-mediated reductive amination was used to convert aldehydes **4a−c** into final compounds **1a−d** (Table 1).[18,19]

Synthesis of the [3-(2,3-Dihydro-1,4-benzodioxin-6-yl)-2-methylphenyl]methanol Derivatives (2a−c). To prepare inhibitors **2a−c**, a multistep synthetic route similar to that for **1a−d** was applied. Compound **5** was obtained by the Suzuki−Miyaura coupling between (3-bromo-2-methylphenyl)-methanol and (2,3-dihydrobenzo[*b*][1,4]dioxin-6-yl)boronic acid. A subsequent Mistunobu etherification reaction between alcohol **5** and an appropiate phenolic aldehyde afforded aldehydes **6a−c**.[21] The sodium cyanoborohydride-mediated reductive amination was used to convert aldehyde **6a** into compound **2a**. Compounds **2b,c** were obtained by the cesium carbonate-promoted O-alkylation of aldehydes **7a,b**, followed by reductive amination using $NaBH_3CN$ and appropriate amines (Table 2).[18,19]

NMR Indicates That 1 and 2 Bind to PD-L1 and Induce Its Oligomerization in Solution. Determination of binding of the lead BMS compounds to PD-L1 was carried out with the $^{1}H-^{15}N$ 2D HMQC NMR spectroscopy on the ^{15}N isotopically enriched domain of human PD-L1 (hPD-L1), which encompassed residues 18−134 of hPD-L1. The ^{15}N-labeled PD-L1 was titrated with increasing concentration of an evaluated compound, and $^{1}H-^{15}N$ 2D HMQC spectra were recorded after addition of each new portion of the compound.[23,24] Ligand-induced chemical shift perturbations in the 2D HMQC spectra confirmed the interaction of **1** and **2** with PD-L1. Additionally, NMR signal doubling in the 2D $^{1}H-^{15}N$ HMQC spectra indicated the K_D of less than 1 μM (and a slow chemical exchange).[25] Moreover, the line width broadening in the 1D proton NMR of PD-L1 suggests that the compounds induce protein oligomerization (Supporting Information Figures S1 and S2), already observed in our recent studies for the (2-methyl-3-biphenylyl)methanol derivative **1c**.[20] The approximate size of the oligomers of all of the small molecule/PD-L1 complexes determined from the NMR analysis is that of a tetramer (Supporting Information Figure S1B). Size exclusion chromatography on PD-L1 in the presence and absence of the inhibitor (**1** and **2**) indicates the **1,2**-induced dimerization of PD-L1 (Supporting Information Figure S3). A single peak corresponding to a protein of molecular weight of 17 kDa was observed for apo-PD-L1, indicating a monomeric form in solution. In the presence of the compound the movement of the peak to shorter retention time confirmed the dimeric state of the complexed PD-L1 (34 kDa) (Supporting Information Figure S3). The X-ray structural data below indicate that the principal oligomerization component of the **1,2**/PD-L1 complexes is dimeric (although the hPD-L1/**1a** complex contains four protein molecules organized into two dimers in the asymmetric unit, the molar ratio of the protein to ligand being 4:2; see below). We have repeated the NMR experiments at lower concentrations to those standards used above (data not shown). At the concentrations of PD-L1 of 0.5 μM, there is a clear-cut large increase of the proton NMR line widths at the molar concentration ratio protein to ligand 4:1, which is identical to that seen in the Supporting Information Figures S1B. We conclude that, at least, at high μM concentrations of PD-L1, NMR monitors the loosely formed tetrameric states of the **1,2**/PD-L1 complexes. However, size exclusion chromatography and X-ray indicate that the most stable unit of the **1,2** induced oligomerization of PD-L1 is that of a dimer.

We have in addition synthesized and tested a large number of fragments and intermediates of **1** and **2** that possess the biphenyl core building element. All these structures induced oligomerization of PD-L1 (Supporting Information Table S2).

NMR detects two groups of the compounds that differ in their modes of binding to PD-L1. The $^{1}H-^{15}N$ 2D HMQC NMR spectrum of the **2**-bound ^{15}N uniformly labeled PD-L1 shows increase of number or cross-peaks and extensive peak overlap compared to the spectrum of the monomeric apo-PD-L1 (Supporting Information Figure S4). This is because, as our recent structure of PD-L1 with a similar inhibitor indicates, one inhibitor molecule is located at the interface of the asymmetric dimer (i.e., the stoichiometry, for example, of **1c**; PD-L1 in the complex is 1:2, respectively).[20] The tetrameric state seen in NMR and in the X-ray comprises a symmetric dimer of the **1c**/PD-L1 dimer. Both the binding site of the inhibitor and the intermolecular interactions within the dimer involve the PD-1 interaction surface of PD-L1.[14,20] To simplify the ^{15}N NMR

DOI: 10.1021/acs.jmedchem.7b00293
J. Med. Chem. 2017, 60, 5857−5867

spectra, we prepared the amino acid type selective-labeling PD-L1 (Supporting Information Figure S4). The amino acids chosen for labeling were those involved directly in the binding of PD-L1 to PD-1 and/or **1c** (i.e., tyrosines) and those close to the binding interfaces (valines). We therefore prepared two PD-L1 compounds labeled with ^{15}N-Val and ^{15}N-Tyr (Supporting Information Figure S4).

In all NMR spectra recorded for the [^{15}N-Val]-PD-L1 and [^{15}N-Tyr]-PD-L1 we observed broadening and/or shifts of the HMQC signals of hPD-L1 during the titration. Upon addition of the compound, compared to the apo-PD-L1, the largest perturbation in the positions of the NMR signals was observed for the signal at δ_H = 7.13 ppm and δ_N = 109.9 ppm in the ^{15}N-Val PD-L1 spectrum (Figure 2). Several of the **1** and **2** compounds were checked. Two clearly distinctive patterns of the compound-induced changes in the spectra have been observed. In the first group of the compounds, the differences in chemical shifts between the two ^{15}N valine signals in the dimer complex, compared to the starting signal of the apo-PD-L1, are $\Delta\delta_H$ = 0.8 and $\Delta\delta_N$ = 2.4 ppm (Figure 2A). This group comprises exclusively compounds **1**. The second group, which contains only **2**, showed these differences to be smaller and equal $\Delta\delta_H$ = 0.10/$\Delta\delta_N$ = 0.4 and $\Delta\delta_H$ = 0.25/$\Delta\delta_N$ = 0.8 ppm for **2a** and **2b**, respectively (Figure 2B).

A similar pattern of grouping was observed for one of the resonances in the spectra of the ^{15}N-Tyr labeled hPD-L1 (the signal at δ_H = 8.12 and δ_N = 116.5) upon titration with tested compounds, but the changes in chemical shift were smaller, approximately $\Delta\delta_H$ = 0.50 and $\Delta\delta_N$ = 1.7 ppm (date not shown). On the basis of the NMR results for the ^{15}N Val-PD-L1, we concluded that these two groups of compounds might differently interact with PD-L1. The representatives of these two groups have therefore been subjected to crystallization, which indeed showed their different extend of binding to hPD-L1.

Structural Basis of the Interaction of 1a and 2a with PD-L1. The crystal structures of **1a** and **2a** in complex with hPD-L1 have been determined to a resolution of 2.35 and 1.7 Å, respectively (Supporting Information Table S3). The structures follow the stoichiometry and molecule arrangement presented lately by us (PDB codes 5J89, 5J8O),[20] nonetheless with novel details leading to the discovery of the hPD-L1s interaction surface subsites highly vulnerable for ligand-induced changes (Figure S5). The asymmetric unit of the hPD-L1/**2a** complex contained one dimer exhibiting a pseudo 2-fold rotational symmetry around an axis parallel to the long axis of the protein molecule. The hPD-L1/**1a** complex crystallized in different configuration with an asymmetric unit containing four protein molecules organized into two dimers rotated 180° around a horizontal axis, with the C-termini of each dimer molecule close to another. In both structures each dimer is harboring one inhibitor in the center of interface of each dimer. Each of the **1a** and **2a** molecules are arranged perpendicular to the long axis of protein, and its location is explicitly occluding the hPD-1 binding site in both hPD-L1 protein molecules, thereby providing a rationale for disrupting the PD-1/PD-L1 interaction.

The **1a**/PD-L1 complex represents the inhibitor-binding mode reported by us in the previous publication.[20] The compound is located in a deep, hydrophobic cleft with roughly cylindrical shape in the cross section. The binding cleft is closed from one side by side chain $_A$Tyr56 which creates the T-stacking interaction with a distal phenyl moiety of the inhibitor and an additional $\pi-\sigma$ and $\pi-$alkyl interactions with $_B$Ala121 and $_A$Met115, respectively (the protein molecules are annotated by subscripts A, B, C, and D according to the chain arrangement in the crystal structure; the inhibitor disposition is described here based on the AB dimer and is similar in the CD dimer unless noted otherwise, Figure 3C, Supporting Information Figure S6). The methyl phenyl ring, rotated around 45° with respect to the distal phenyl ring, located in the center of the cleft is stabilized by hydrophobic interactions with both A (methyl group) and $_B$Met115 (ring and methyl group) with additional contacts with $_A$Ala121 side chain. The 1,3-dimethoxyphenyl group, connected with the methyl-phenyl ring through the ether bond, which is close to the solvent accessible part of the cleft, interacts with $_B$Tyr56 through the $\pi-\pi$ stacking, thereby providing strong stabilization for this part of the inhibitor with minor contribution from hydrophobic interactions with the side chain of $_A$Asp122. The *N*-(2-aminoehtyl)acetamide tail creates a hydrogen bond with $_B$Gln66 and $_A$Asp122 (Figure 3A–C, Supporting Information Figures S7 and S8).

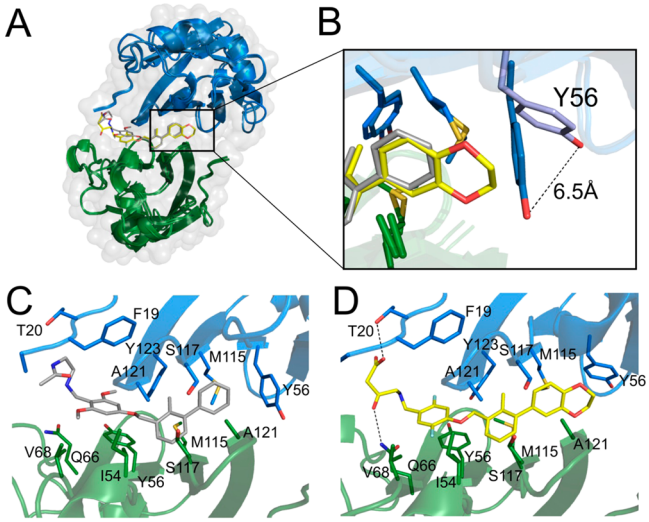

Figure 3. Cocrystal X-ray structures of **1a** and **2a** bound to human PD-L1. White (A) overlay of the **1a**/PD-L1 and **2a**/PD-L1 structures demonstrates that **1a** (gray) and **2a** (yellow) bind to the dimeric PD-L1 (mixed ribbon/surface representation) with different binding modes. The PD-L1 molecules are colored blue and green for chains A and B, respectively. (B) Close-up view of the movement $_A$Tyr56 (violet) that is induced by the 2,3-dihydro-1,4-benzdioxine group of **2a** (yellow) compared with the $_A$Tyr56 (gray) arrangement in the complex of **1a**/PD-L1. The movement of $_A$Tyr56 makes the binding pocket of PD-L1 accessible to solvent on both sides, changing a deep hydrophobic cleft into the deep, hydrophobic tunnel. (C) Detailed interactions of **1a** (gray) at the binding cleft of PD-L1. Compound **1a** binds at a hydrophobic cavity formed upon the PD-L1 dimerization. Color coding as in (A). (D) Detailed interactions of **2a** (yellow) at the binding cleft of PD-L1. **2a** binds at a hydrophobic tunnel formed upon the PD-L1 dimerization; the movement of the aromatic ring of $_A$Tyr56, which is induced by the 2,3-dihydro-1,4-benzdioxine moiety, is highlighted. Color coding as in (A).

The **2a** inhibitor is located perpendicularly to the C, F, and G strands of PD-L1, creating the interface similar to that of the PD-1 interacting surface (canonical Ig-strand designations are used; Figure S9). The linear arrangement of the compound accommodates it into a 16 Å long, cylindrical, hydrophobic tunnel between two hPD-L1 monomers. The 2,3-dihydro-1,4-

DOI: 10.1021/acs.jmedchem.7b00293
J. Med. Chem. 2017, 60, 5857–5867

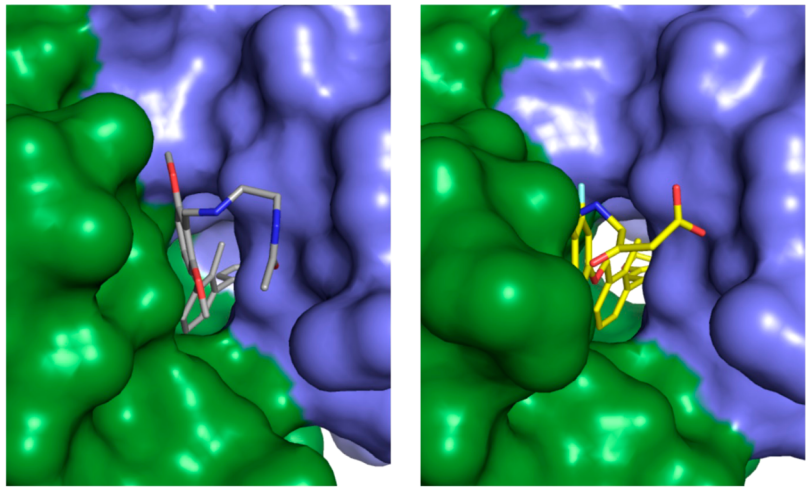

Figure 4. Comparison between the hydrophobic, cylindrical pocket of PD-L1 accommodating **1a** (gray) (left panel) and the extended deep hydrophobic tunnel formed by **2a** (yellow) upon binding with its target protein (right panel). The PD-L1 molecule (surface representation) are colored blue and green for chain A and chain B, respectively.

benzodioxinyl group of **2a** provokes movement of the $_{A}$Tyr56 C(β)−C(γ) by 77° around the C(α)−C(β) axis, making this part of the compound accessible for the solvent and thereby changing deep hydrophobic cleft into deep, hydrophobic tunnel (Figures 3 and 4, Supporting Information Figures S7, S8, and S10). The most distal ring of **2a** interacts with $_{A}$Ala121 through a 2.1 Å long hydrogen bond and $\pi-\sigma$ interaction with $_{A}$Tyr56, while its second ring (hidden deeper in the tunnel) provides additional hydrophobic contacts with $_{A}$Met115 and $_{B}$Ala121 (π−alkyl and $\pi-\sigma$, respectively). The central methyl phenyl ring is rotated roughly around 45° to the plane of the 2,3-dihydro-1,4-benzodioxinyl moiety with the methyl group pointing toward chain A with major interactions involving the hydrophobic contacts with Met115 of the chain A and B and $_{A}$Ala121. Alkyl interactions with $_{A}$Tyr123 are also present providing more rigid arrangement of the compound between PD-L1 chains. The substituted 2,5-difluorophenyl ring of **2a** is stabilized mostly through $\pi-\pi$ stacking interaction with $_{B}$Tyr56 ring with minor contribution from the halogen bonding between fluorine atom and $_{A}$Asp122. Additionally, (*S*)-4-amino-3-hydroxybutyric acid moiety of **2a** creates two hydrogen bonds with $_{A}$Thr20 and $_{B}$Gln66 (Figure 3D, Supporting Information Figures S8 and S11).

DISCUSSION

Several crystal structures of the antibodies complexed with both PD-1 and PD-L1 have been determined, revealing the structural basis of the antibody-based immune checkpoint blockade.[26] Crystal structures of the anti-PD-1 pembrolizumab Fab fragment complexed with hPD-1 (PDB code 5GGS) and PD-1 in complex with nivolumab Fab (PDB code 5GGR) have showed that the mechanisms of their interaction are highly similar because of partially shared epitopes. Structures of the fully human IgG4 antibody (the Fab protein BMS-936559 from Bristol-Myers Squibb) (PDB code 5GGT) and the avelumab single chain Fv fragment (scFv) (PDB code 5GRJ) complexed with PD-L1 were also determined.[27−31] Additionally, ultrahigh-affinity mutants of PD-1 were described.[31,32] The mutant by Maute et al.,[29] termed the high-affinity consensus (HAC) PD-1, exhibits a 35 000-fold enhanced affinity for PD-L1 in comparison to the wild-type protein. Structure of the complex of an (HAC) PD-1 mutant bound to hPD-L1 was also determined, providing the structural and biophysical basis for enhanced binding of these proteins.[33]

Compared to the antibodies, conspicuously missing from this class of therapies are traditional small-molecule drugs. Although small-molecule pharmacological modulators of the PD-1/PD-L1 axis are highly awaited, to date only a few series of small molecules, macrocyclic peptides, peptides, or peptidomimetics targeting this interaction were reported.[15−17] Among them the group of entirely small-molecule compounds based on the hydrophobic biphenyl core scaffold has been described recently by Bristol-Myers Squibb.[18,19] We provided structural basis of interactions between two examples of compounds **1b,c** with PD-L1, evidencing that PD-1/PD-L1 axis may be targeted not only by mAbs but also by small molecules.[20] In the present study we describe two new crystal structures of compounds **1a** and **2a**, both bound to the dimeric PD-L1. Surprisingly, the binding mode of inhibitor **2a**, which contains the 2,3-dihydro-1,4-benzodioxinyl group, significantly differs from that of **1a** and those reported by us previously (**1b,c**) (PDB codes 5J89, 5J8O) (Supporting Information Figure S5). Our structural data show that inhibitor **2a** upon binding to PD-L1 induces conformational changes in PD-L1, showing the ligand binding site of PD-L1 to be more flexible than it was previously seen. This quite unexpected formation of the hydrophobic tunnel, induced by the 2,3-dihydro-1,4-benzdioxinyl group of **2a**, redefines the described pharmacophore model and creates new possibilities for further design of PD-L1 inhibitors (Figures 3 and 4).[20] The formation of the tunnel is associated with the movement of the aromatic ring of $_{A}$Tyr56.

We also partition **1**,**2**-like large ligands (MW ≈ 600) into smaller fragments and screen the resulting fragments for binding to PD-L1. All these structures have shown binding to PD-L1, albeit weaker. They induce dimerization of PD-L1, indicating that this structural part of the compounds is most likely involved in dimerization (Supporting Information Table S2). These initial small derivative fragments, with indication of binding properties at the site of interest determined by the NMR ^{1}H−^{15}N HMQC titration, could be used to construct libraries of larger structures, which can be submitted to the same ^{1}H−^{15}N HMQC titration experiments in the future.

DOI: 10.1021/acs.jmedchem.7b00293
J. Med. Chem. 2017, 60, 5857−5867

EXPERIMENTAL SECTION

Gel Filtration Experiment. A Superdex S75 10/30 HR column was equilibrated with buffer containing 10 mM Tris and 20 mM NaCl. Protein was concentrated to 3 mg/mL, and 200 μL of sample was loaded onto the column (apo-hPD-L1 separation). In the case of the hPD-L1/inhibitor complexes, the protein at the 3 mg/mL concentration was mixed with the inhibitor in 3:1 (inhibitor/protein) molar ratio, centrifuged for 10 min at 15 000*g* and 200 μL of resulting supernatant was loaded onto the column.

Protein Expression and Purification. The proteins was expressed and purified as described earlier.[20] Briefly, hPD-L1 (residues 18−134) was expressed in *E. coli* BL21 (DE3) as inclusion bodies. After bacteria collection, the pellet was washed and the obtained inclusion bodies were dissolved in the GuHCl buffer. Refolding was performed by a dropwise dilution in buffer containing 1 M L-arginine, 100 mM Tris, pH 8.0, 2 mM EDTA, 0.25 mM reduced glutathione, and 0.25 mM oxidized glutathione. After refolding, protein was dialyzed against 10 mM Tris, pH 8.0, containing 20 mM NaCl three times, concentrated, and purified using a Superdex S75 gel filtration column equilibrated with 10 mM Tris, pH 8.0, containing 20 mM NaCl.

Crystallization of the hPD-L1 in Complex with Small Molecule Inhibitor. The purified protein was mixed with **1a** or **2a** in 3:1 (inhibitor/protein) molar ratio, concentrated to 5 mg/mL, and the crystallization screening was carried out. Diffraction-quality crystals were obtained at room temperature from the conditions containing 0.1 M Tris, pH 8.5, 0.2 M magnesium chloride, 30% (w/v) PEG 4000, and 0.01 M Tris, pH 8.4, 0.28 M sodium chloride, 27% (w/v) PEG 4000 for **1a** and **2a**, respectively.

Crystal Structure Determination. The crystals were flash-cooled in liquid nitrogen without cryoprotection. The diffraction data were collected at the Helmholtz Centrum 14.1 beamline at BESSY (Berlin, Germany).[34] The data were indexed and integrated using XDS,[35,36] scaled and merged using Aimless.[37] The initial phases were obtained by molecular replacement using Phaser and code 5C3T as a search model.[38] The models were manually built in the resulting electron density maps using Coot.[39] Restrained refinement was performed using Phenix.[40]

NMR Experiments. Uniform ^{15}N labeling was obtained by expressing the proteins in the M9 minimal medium containing $^{15}NH_4Cl$ as the sole nitrogen source. For NMR measurements the buffer was exchanged by gel filtration to PBS pH 7.4 (hPD-L1) or 25 mM sodium phosphate containing 100 mM NaCl, pH 6.4 (hPD-1). 10% (v/v) of D_2O was added to the samples to provide lock signal. All spectra were recorded at 300 K using a Bruker Avance 600 MHz spectrometer. Binding of the compounds was analyzed by titrating the ^{15}N-labeled PD-L1 (0.11 mM) and recording the ^1H and $^1H-^{15}N$ HMQC spectra prior to after addition of the compound. The approximate molecular weights of protein populations present in the sample were determined by analyzing the line width (relaxation time) of well separated NMR signals.

General Chemistry. The compounds were synthesized as shown in Tables 1 and 2 according to the procedures similar to those described in the disclosures.[18,19] All reagents were obtained from Sigma-Aldrich and used without additional purification unless noted otherwise. NMR spectra were recorded on Bruker Avance 600 MHz spectrometer. All chemical shifts (δ) are reported in ppm and coupling constants (J) in Hz. All chemical shifts are related to the solvent peaks (DMSO-d_6, $CDCl_3$). Infrared spectra were recorded for the solid samples on a Nicolet IR200 spectrometer using ATR technique. High-resolution mass spectrometry (HRMS) spectra were recorded on a microTOF-QII apparatus using the ESI ionization mode. Flash chromatography was performed on the Grace Reveleris X2 flash chromatography system with the Grace Resolv silica cartridges. Elemental analyses were performed on a Vario Micro Cube apparatus. The UPLC−MS experiments were carried out on the TQD Waters H-Class spectrometer (column ACQUITY UPLC BEH C18 1.7 μm, 2.1 mm × 50 mm, method, 6 min, gradient 0−3 min 80% H_2O to 20% MeCN, 3−3.5 min 100% MeCN, 3.5−6 min 80% H_2O to 20% MeCN). Purities of all final compounds (determined using chromatographic UPLC or elemental analysis) were 95% or higher. Thin-layer chromatography (TLC) was performed on TLC silica plates (60 F_{254}) and visualized with ultraviolet light at 254 nm. Melting points were determined with an Ascon-M5 apparatus. Details are given in Supporting Information.

*N-{2-[({2,6-Dimethoxy-4-[(2-methyl-3-phenylphenylmethoxy]-phenyl}methyl)amino]ethyl}acetamide Hydrochloride (**1a**).* A solution of **4a** (90 mg, 0.25 mmol), *N*-(2-aminoethyl)acetamide (104 mg, 1.02 mmol), sodium cyanoborohydride (83.5 mg, 1.3 mmol), and AcOH (2 drops) in DMF (5 mL) was stirred at 80 °C for 3 h. The mixture was concentrated under reduced pressure. Purification by flash chromatography (0−60% MeOH in $CHCl_3$) provided the product as colorless solid (41 mg, yield 36%). ^1H NMR (600 MHz, DMSO-d_6) δ: 7.75 (t, J = 5.4 Hz, 1H), 7.47 (dd, J = 7.6, 1.05 Hz, 1H), 7.48−7.45 (m, 2H), 7.39−7.37 (m, 1H), 7.33−7.30 (m, 2H), 7.29 (t, J = 7.6 Hz, 1H), 7.21 (dd, J = 7.6, 1.2 Hz, 1H), 6.36 (s, 2H), 5.15 (s, 2H), 3.76 (s, 6H), 3.59 (s, 2H), 3.08 (q, J = 6.3 Hz, 2H), 2.43 (t, J = 6.4 Hz, 2H), 2.22 (s, 3H), 1.77 (s, 3H) ppm. ^{13}C NMR (151 MHz, DMSO-d_6) δ: 169.0, 159.2, 158.9, 142.2, 141.4, 135.6, 134.0, 129.7, 129.2, 128.2, 127.0, 125.5, 108.7, 91.5, 68.6, 55.7, 47.9, 40.5, 40.1, 38.8, 22.6, 15.9 ppm. IR (ATR) 3317, 2934, 2836, 1647, 16155, 1597, 1498, 1200, 1147, 1033 cm^{-1}. HRMS ESI-MS-q-TOF for $C_{27}H_{32}N_2O_4$ $[M + H]^+$ found, 449.2440 m/z; calcd mass, 449.2440. Mp: 112−113 °C. UPLC−MS (DAD/ESI): t_R = 6.11 min, for $C_{27}H_{32}N_2O_4$ $[M + H]^+$ found, 449.20 m/z; calcd mass, 449.24.

*1-({3-Bromo-4-[(2-methyl-3-phenylphenyl)methoxy]phenyl}-methyl)piperidine-2-carboxylic Acid (**1b**).* Compound **1b** was prepared following the protocol for **1a**, using **4b** (150 mg, 0.39 mmol), piperidine-2-carboxylic acid (148 mg, 1.17 mmol), $NaBH_3CN$ (74 mg, 1.17 mmol), and AcOH (2 drops) dissolved in DMF (4 mL). Purification by flash chromatography (0−60% MeOH in EtOAc) provided the product as colorless solid (50 mg, yield 26%). ^1H NMR (300 MHz, DMSO-d_6) δ: 17.45 (br s, 1H), 7.73 (d, J = 2.0 Hz, 1H), 7.55 (dd, J = 7.5, 1.2 Hz, 1H), 7.49−7.35 (m, 8H), 7.22 (dd, J = 7.5, 1.2 Hz, 1H), 5.29 (s, 2H), 4.62 (s, 2H), 3.78 (t, J = 7.0 Hz, 1H), 3.26−3.17 (m, 2H), 2.23 (s, 3H), 2.03−1.93 (m, 2H), 1.86−1.56 (m, 3H), 1.50−1.34 (m, 1H) ppm. ^{13}C NMR (75 MHz, DMSO-d_6) δ: 170.2, 155.7, 137.1, 134.9, 133.8, 133.7, 129.7, 129.2, 128.3, 127.6, 127.0, 125.6, 122.0, 113.7, 110.8, 69.9, 69.4, 68.6, 59.9, 25.0, 20.1, 19.6, 15.8 ppm. IR (ATR) 3329, 2946, 2520, 1728, 1605, 1500, 1452, 1290, 1265, 1056 cm^{-1}. HRMS ESI-MS-q-TOF for $C_{27}H_{28}BrNO_3$ $[M + Na]^+$ found, 516.1137 m/z; calcd mass, 516.1150. Mp: 119−121 °C. UPLC−MS (DAD/ESI): t_R = 6.49 min, for $C_{27}H_{28}BrNO_3$ $[M + H]^+$ found, 494.06 m/z; calcd mass, 494.13.

*N-{2-[({2-Methoxy-6-[(2-methyl-3-phenylphenyl)methoxy]-pyridin-3-yl}methyl)amino]ethyl}acetamide Hydrochloride (**1c**).* Combined sodium cyanoborohydride (200 mg, 3.18 mmol), *N*-(2-aminoethyl)acetamide (250 mg, 2.45 mmol), and **4c** (200 mg, 0.60 mmol) in DMF (20 mL) and AcOH (5 drops) were stirred at room temperature for 16 h. The mixture was concentrated under reduced pressure. The product was purified by flash chromatography on silica gel (0−60% MeOH in EtOAc) to give the product as a yellow oil. The product was converted into the corresponding hydrochloride salt and recrystallized from acetone (76 mg, yield 27%). ^1H NMR (600 MHz, DMSO-d_6) δ: 8.97 (br s, 2H), 8.20 (t, J = 5.6 Hz, 1H), 7.82 (d, J = 8.0 Hz, 1H), 7.47−7.44 (m, 3H), 7.39−7.36 (m, 1H), 7.31−7.30 (m, 2H), 7.21 (t, J = 7.6, 1H), 7.19 (dd, J = 7.7, 1.2 Hz, 1H), 6.53 (d, J = 8.0 Hz, 1H), 5.45 (s, 2H), 4.04 (s, 2H), 3.95 (s, 3H), 3.36 (q, J = 6.3 Hz, 2H), 2.95 (t, J = 6.3 Hz, 2H), 2.22 (s, 3H), 1.83 (s, 3H) ppm. ^{13}C NMR (151 MHz, DMSO-d_6) δ: 170.2, 162.5, 160.5, 144.0, 142.2, 141.4, 135.6, 133.9, 129.7, 129.2, 128.3, 128.3, 127.0, 125.5, 105.3, 101.5, 66.5, 53.7, 46.1, 44.1, 35.2, 22.6, 15.9 ppm. IR (ATR) 3253, 3062, 2934, 2702, 1651, 1605, 1587, 1463, 1309, 1003 cm^{-1}. HRMS ESI-MS-q-TOF for $C_{25}H_{29}N_3O_3$ $[M + H]^+$ found, 420.2299 m/z; calcd mass, 420.2287. Mp: 139−140 °C. UPLC−MS (DAD/ESI): t_R= 5.79 min, for $C_{25}H_{29}N_3O_3$ $[M + H]^+$ found, 420.22 m/z; calcd mass, 420.23.

*(2R)-2-[({2,6-Dimethoxy-4-[(2-methyl-3-phenylphenyl)methoxy]-phenyl}methyl)amino]-3-methylbutan-1-ol Hydrochloride (**1d**).*

DOI: 10.1021/acs.jmedchem.7b00293
J. Med. Chem. 2017, 60, 5857−5867

Compound **1d** was prepared according to the protocol of **1a**, using **4a** (181 mg, 0.5 mmol), L-valinol (210 mg, 2.03 mmol), $NaBH_3CN$ (167 mg, 2.6 mmol), and AcOH (2 drops) in DMF (4 mL). The residue was purified by silica gel flash chromatography (0−60% MeOH in EtOAc). After conversion into the corresponding hydrochloride salt product was recrystallized from isopropanol and diisopropyl ether (55 mg, yield 48%). ^{1}H NMR (600 MHz, DMSO-d_6) δ: 8.08 (br d, J = 54.5 Hz, 2H), 7.5 (dd, J = 6.6, 1.0 Hz, 1H), 7.46−7.43 (m, 2H), 7.38−7.35 (m, 1H), 7.31−7.27(m, 3H), 7.21 (dd, J = 6.6, 1.2 Hz, 1H), 6.46 (s, 2H), 5.34 (t, J = 4.9 Hz, 1H), 5.21 (s, 2H), 4.12 (t, J = 5.6 Hz, 2H), 3.83 (s, 6H), 3.72−3.68 (m, 1H), 2.80−2.75 (m, 1H), 2.22 (s, 3H), 2.09−2.06 (m, 1H), 1.23 (s, 1H), 0.96 (d, J = 6.9 Hz, 3H), 0,92 (d, J = 6.9 Hz, 3H) ppm. ^{13}C NMR (151 MHz, DMSO-d_6) δ: 161.9, 159.9, 142.7, 141.8, 135.8, 134.6, 130.3, 129.6, 128.8, 128.7, 127.5, 126.0, 100.2, 92.0, 69.3, 67.8, 64.5, 57.7, 56.5, 38.7, 26.8, 23.3, 19.6, 18.1, 16.4 ppm. IR (ATR) 3289 (br), 2965, 1611, 1595, 1463, 1150 cm^{-1}. HRMS ESI-MS-q-TOF for $C_{28}H_{35}NO_4$ $[M + H]^+$ found, 450.2640 m/z; calcd mass, 450.2644. Mp: 74−76 °C. UPLC−MS (DAD/ESI): t_R = 6.68 min, for $C_{28}H_{35}NO_4$ $[M + H]^+$ found, 450.20 m/z; calcd mass, 450.26.

*(3S)-4-{[(4-{[3-(2,3-Dihydro-1,4-benzodioxin-6-yl)-2-methylphenyl]methoxy}-2,5-difluorophenyl)methyl]amino}-3-hydroxybutanoic Acid Hydrochloride (**2a**).* Compound **2a** was prepared following the protocol for **1a**, using **6a** (396 mg, 1.0 mmol), (*S*)-4-amino-3-hydroxybutanoic acid (224 mg, 2.0 mmol), $NaBH_3CN$ (333 mg, 5.3 mmol), AcOH (3 drops) in DMF (10 mL). After purification by gel flash chromatography (0−60% MeOH in $CHCl_3$) the product was converted into the corresponding hydrochloride salt and recrystallized from diethyl ether and ethanol (192 mg, yield 36%). ^{1}H NMR (600 MHz, $CDCl_3$ δ: 7.39−7.37 (m, 1H), 7.24−7.22 (m, 2H), 7.06 (dd, $^{3,4}J_{H-F}$ = 10.9, 6.9 Hz, 1H), 6.90 (d, 8.2 Hz, 1H), 6.82 (d, J = 2.1 Hz, 1H), 6,79 (dd, $^{3,4}J_{H-F}$ = 10.9, 6.8 Hz, 1H), 6.77 (dd, J = 8.2, 2.1 Hz, 1H), 5.11 (s, 2.0, 2H), 4.54−4.50 (m, 1H), 4.48 (d, J = 14.8 Hz, 1H), 4.43 (d, J = 14.8 Hz, 1H), 4.30 (s, 4H), 3.57 (dd, J = 10.8, 5.5 Hz, 1H), 3.26 (dd, J = 10.8, 1.2 Hz, 1H), 2.73 (dd, J = 17.4, 6.7 Hz, 1H), 2.43 (dd, J = 17.4, 2.2 Hz, 1H), 2.26 (s, 3H), 1.27 (d, J = 5.5 Hz, 1H) ppm. ^{13}C NMR (151 MHz, $CDCl_3$) δ: 172.8, 156.7 (d, $^1J_{C-F}$ = 242.9 Hz), 149.3 (d, $^1J_{C-F}$ = 242.4 Hz), 147.3, 147.2, 147.1, 143.2, 142.8, 142.6, 135.3, 134.6, 134.2, 130.6, 127.8, 125.7, 122.7, 118.4, 117.3, 117.1 (dd, $^{2,3}J_{C-F}$ = 20.8, 5.5 Hz), 117.0, 115.2 (dd, $^{2,3}J_{C-F}$ = 17.5, 5.5 Hz), 103.5, 103.4, 71.0, 70.9, 70.9, 64.7, 64.6, 55.9, 41.2, 39.2, 16.3 ppm. HRMS ESI-MS-q-TOF for $C_{27}H_{27}F_2NO_6$ $[M - H_2O + Na]^+$found, 504.1625 m/z; calcd mass, 504.1598. Mp: 82−83 °C. UPLC−MS (DAD/ESI): t_R = 6.87 min, for $C_{27}H_{27}F_2NO_6$ $[M - OH]^+$ found, 482.18 m/z; calcd mass, 482.16.

*(2R)-2-[({2-[(3-Cyanophenyl)methoxy]-4-{[3-(2,3-dihydro-1,4-benzodioxin-6-yl)-2-methylphenyl]methoxy}-5-methylphenyl}methyl)amino]-3-hydroxypropanoic Acid Hydrochloride (**2b**).* Compound **2b** was prepared according to the protocol of **1a**, using **7a** (140 mg, 0.3 mmol), D-serine (116 mg, 1.1 mmol), $NaBH_3CN$ (91 mg, 1.4 mmol), and AcOH (2 drops) in DMF (4 mL). The residue was purified by silica gel flash chromatography (0−60% MeOH in EtOAc). The product was converted into the corresponding hydrochloride salt and recrystallized from methanol (62 mg, yield 40%). ^{1}H NMR (600 MHz, DMSO-d_6) 8.03 (s, 1H), 7.91 (d, J = 7.8 Hz, 1H), 7.81 (dt, J = 7.8, 1.2 Hz, 1H), 7.61 (t, J = 7.8 Hz, 1H), 7,41 (dd, J = 7.8, 0.8 Hz, 1H), 7.23 (t, J = 7.8 Hz, 1H), 7.19 (s, 1H), 7.16 (dd, J = 7.7, 1.0 Hz, 1H), 6.93 (s, 1H), 6.92 (d, J = 8.2 Hz, 1H), 6.79 (d, J = 2.1 Hz, 1H), 6.75 (dd, J = 8.2, 2.1 Hz, 1H), 5.30 (d, J = 12.6 Hz, 1H), 5.26 (d, J = 12.6 Hz, 1H), 5.14 (s, 2H), 4.28 (s, 4H), 4.09 (d, J = 13.0 Hz, 1H), 4.02 (d, J = 13.0 Hz, 1H), 3.77 (dd, J = 11.4, 6.6 Hz, 1H), 3.66 (dd, J = 11.4, 6.6 Hz, 1H), 3.24−3.21 (m, 2H), 2.22 (s, 3H), 2.10 (s, 3H) ppm. ^{13}C NMR (151 MHz, DMSO-d_6) δ: 168.5, 157.5, 155.5, 143.0, 142.5, 138.6, 133.9, 132.5, 131.7, 131.1, 129.7, 129.6, 127.4, 125.5, 122.1, 118.7, 118.0, 117.7, 116.8, 111.5, 98.4, 68.9, 68.7, 64.3, 61.8, 60.1, 45.0, 15.9, 15.3 ppm. IR (ATR) 3637, 3080 (br), 2928, 2880, 2230, 1616, 1506, 1448, 1313, 1279, 1125, 1052, 792 cm^{-1}. HRMS ESI-MS-q-TOF for $C_{35}H_{34}N_2O_7$ $[M + Na]^+$ found, 617.2278 m/z; calcd mass, 617.2264. Mp: 153.5−154.5 °C. UPLC−MS (DAD/ESI): t_R = 6.47 min, for $C_{35}H_{34}N_2O_7$ $[M + H]^+$ found, 595.25 m/z; calcd mass, 595.24.

*(2R,4R)-1-({5-Chloro-2-[(3-cyanophenyl)methoxy]-4-{[3-(2,3-dihydro-1,4-benzodioxin-6-yl)-2-methylphenyl]methoxy}phenyl}methyl)-4-hydroxypyrrolidine-2-carboxylic Acid Hydrochloride (**2c**).* Compound **2c** was prepared following the protocol for **1a**, using **7b** (230 mg, 0.4 mmol), (2*R*,4*R*)-4-hydroxypyrrolidine-2-carboxylic acid (262 mg, 2.0 mmol), sodium cyanoborohydride (145 mg, 2.3 mmol), AcOH (3 drops) in DMF (4 mL). After purification by flash chromatography (0−60% MeOH in EtOAc) the product was converted into the hydrochloride salt and recrystallized from isopropanol (62 mg, yield 40%). ^{1}H NMR (600 MHz, DMSO-d_6) δ: 7.98 (s, 1H), 7.88 (d, J = 8.1 Hz, 1H), 7.83 (dt, J = 7.8, 1.3 Hz, 1H), 7.62 (t, J = 7.8 Hz, 1H), 7.48−7.42 (m, 2H), 7.24 (t, J = 7.6 Hz, 1H), 7.18 (dd, J = 7.6 Hz, 1H), 7.1 (s, 1H), 6.92 (d, J = 8.1 Hz, 1H), 6.78 (d, J = 2.11 Hz, 1H), 6.75 (dd, J = 8.2, 2.1 Hz, 1H), 5.31 (d, J = 12.5 Hz, 1H), 5.29 (d, J = 12.5 Hz, 1H), 5.23 (s, 2H), 4.28 (s, 4H), 4.22−4.18 (m, 1H), 3.95 (d, J = 13.2 Hz, 1H), 3.80 (d, J = 13.2 Hz, 1H), 3.41−3.39 (m, 1H), 2.95 (d, J = 10.6 Hz, 1H), 2.71 (dd, J = 10.6, 4.9 Hz, 1H), 2.34 (ddd, J = 13.2, 9.7, 5.8 Hz, 1H), 2.24 (s, 3H), 1.84 (br d, J = 13.2 Hz, 1H) ppm. ^{13}C NMR (151 MHz, DMSO-d_6) δ: 172.6, 155.9, 153.4, 143.0, 142.5, 138.4, 135.0, 134.4, 134.0, 132.5, 131.8, 131.5, 131.1, 129.9, 125.6, 122.06, 118.7, 117.7, 116.8, 113.0, 111.5, 100.5, 69.7, 69.0, 68.6, 64.1, 62.0, 61.0, 51.5, 38.2, 15.8 ppm. IR (ATR) 3270, 2966, 2230, 1633, 1607, 1507, 1312, 1166, 1067 cm^{-1}. HRMS ESI-MS-q-TOF for $C_{36}H_{33}ClN_2O_7$ $[M + Na]^+$ found, 663.1855 m/z; calcd mass, 641.21. Mp: 81−83 °C. UPLC−MS (DAD/ESI): t_R = 6.51 min, for $C_{36}H_{33}ClN_2O_7$ $[M + H]^+$ found, 641.16 m/z; calcd mass, 641.21.

*(2-Methyl-3-biphenylyl)methanol (**3**).* A mixture of (3-bromo-2-methylphenyl)methanol (4.6 g, 22.8 mmol), phenylboronic acid (5.7 g, 46.3 mmol), and Pd(dppf)Cl_2·DCM (0.2 g, 0.1 mmol) in toluene (34.5 mL) and ethanol (11.3 mL) was placed under argon. To this solution sodium bicarbonate, 2 M (34.5 mL, 69.0 mmol) was added and the mixture was heated at 80 °C for 30 min. Ethyl acetate (44 mL) and (11 mL) water were added to the reaction mixture. The organic extract was concentrated by rotatory evaporation. The crude product was chromatographed on silica gel, eluting with 0−40% EtOAc in hexane to afford 4.6 g (yield 98%) of an off-white solid. ^{1}H NMR (600 MHz, $CDCl_3$) δ: 7.43−7.49 (m, 3H), 7.37−7.34 (m, 1H), 7.31−7.29 (m, 2H), 7.47−7.44 (m, 3H), 7.26 (t, J = 7.5 Hz, 1H), 7.20 (dd, J = 7.6, 1.3 Hz, 1H), 4.78 (s, 2H), 2.25 (s, 3H) ppm. ^{13}C NMR (151 MHz, $CDCl_3$) δ: 143.0, 142.2, 140.0, 133.8, 129.7, 129.5, 128.2, 127.0, 126.9, 125.7, 64.2, 16.0 ppm. IR (ATR): 3365, 3054, 1601, 1469, 1047, 757 cm^{-1}. Mp: 58−59 °C. UPLC−MS (DAD/ESI): t_R= 6.35 min, for $C_{14}H_{14}O$ $[M - OH]^+$ found, 181.03 m/z; calcd mass, 181.11

*2,6-Dimethoxy-4-[(2-methyl-3-phenylphenyl)methoxy]-benzaldehyde (**4a**).* To the ice-cooled solution of 2,6-dimethoxy-4-[(2-methyl-3-phenylphenyl)methoxy]benzaldehyde (0.92 g, 5.04 mmol), triphenylphosphine (1.45 g, 5.55 mmol), and **3** (1.0 g, 5.04 mmol) in dry THF (21 mL), DIAD (1.08 mL, 5.55 mmol) in THF (21 mL) was added dropwise. The resulting yellow solution was allowed to warm to room temperature and stirred for additional 20 h. The mixture was concentrated under reduced pressure. Purification by flash chromatography (0−60% EtOAc in hexane) yielded **4a** (1.02 g, 56%) as a colorless solid. ^{1}H NMR (600 MHz, DMSO-d_6) δ: 10.37 (s, 1H), 7.44−7.40 (m, 3H), 7.38−7.35 (m, 1H), 7.32−7.28 (m, 4H), 6.20 (s, 2H), 5.16 (s, 2H), 3.89 (s, 6H), 2.27 (s, 3H) ppm. ^{13}C NMR (151 MHz, DMSO-d_6) δ: 187.9, 165.6, 164.3, 143.4, 141.9, 134.7, 134.3, 130.8, 129.5, 128.5, 128.3, 127.1, 125.9, 109.1, 91.1, 69.7, 56.2, 16.4 ppm. IR (ATR) 3013, 2936, 1668, 1607, 1607, 1582, 1465, 1166 cm^{-1}. HRMS ESI-MS-q-TOF for $C_{23}H_{22}O_4$ $[M + Na]^+$ 385.1420 m/z; calcd mass, 385.1416. Mp: 161.5−162 °C. UPLC−MS (DAD/ESI): t_R = 8.08 min, for $C_{23}H_{22}O_4$ $[M + H]^+$ found, 363.13 m/z; calcd mass, 363.16.

*3-Bromo-4-[(2-methyl-3-phenylphenyl)methoxy]benzaldehyde (**4b**).* Compound **4b** was prepared as described for **4a**, using 3-bromo-4-hydroxybenzaldehyde (0.71 g, 3.51 mmol), PPh_3 (1.02 g, 3.89 mmol), **3** (0.70 g, 0.52 mmol) dissolved in THF (21 mL), and solution of DIAD (0.74 mL, 3.89 mmol) in THF (21 mL). The residue was purified by flash chromatography on silica gel using 0−60% EtOAc in hexane. Recrystallization from MeOH yielded colorless

DOI: 10.1021/acs.jmedchem.7b00293
J. Med. Chem. 2017, 60, 5857−5867

solid (0.47 g, yield 35%). ^{1}H NMR (600 MHz, DMSO-d_6) δ: 9.87 (s, 1H), 8.14 (d, J = 2.0 Hz, 1H), 7.97 (dd, J = 6.5, 2.0 Hz, 1H), 7.55−7.52 (m, 2H), 7.48−7.45 (m, 2H), 7.40−7.37 (m, 1H), 7.33−7.30 (m, 3H), 7.22 (dd, J = 6.5 Hz, 1H), 5.39 (s, 2H), 2.23 (s, 3H) ppm. ^{13}C NMR (151 MHz, DMSO-d_6) δ: 190.6, 159.2, 142.2, 141.2, 134.6, 134.0, 133.9, 131.2, 130.8, 129.8, 129.2, 128.3, 127.5, 127.0, 125.6, 114.1, 111.9, 69.8, 15.9 ppm. IR (ATR) 3063, 2852, 1689, 1594, 1278, 1254, 1189, 1048 cm^{-1}. HRMS ESI-MS-q-TOF for $C_{21}H_{17}BrO_2$ [M + Na]$^+$ found, 403.0302 m/z; calcd mass, 403.0310. Mp: 101−102 °C. UPLC−MS (DAD/ESI): t_R = 9.17 min, for $C_{21}H_{17}BrO_2$ [M + H]$^+$ found, 381.00 m/z; calcd mass, 381.05.

*2-Methoxy-6-[(2-methyl-3-phenylphenyl)methoxy]pyridine-3-carbaldehyde (**4c**).* Palladium(II) acetate (0.08 g, 0.36 mmol), Cs_2CO_3 (2.23 g, 6.83 mmol), *t*-BuXPhos (0.29 g, 0.68 mmol), 2-chloro-6-methoxy-3-pyridinecarboxaldehyde (0.59 g, 3.41 mmol), **3** (0.88 g, 4.44 mmol), and toluene (30 mL) were combined and purged by a stream of argon for 3 min. The reaction was sealed and heated at 80 °C for 4 h. The mixture was filtered through a pad of Celite. The filtrate was concentrated under reduced pressure. The product was purified by flash chromatography on silica gel using 0−60% EtOAc in hexane. The product was recrystallized from diethyl ether (488 mg, 35%). ^{1}H NMR (600 MHz, $CDCl_3$) δ: 10.22 (d, J = 0.8 Hz, 1H), 8.06 (d, J = 8.4 Hz, 1H), 7.44−7.41 (m, 3H), 7.37−7.34 (m, 1H), 7.32−7.30 (m, 2H), 7.28 (d, J = 7.5 Hz, 1H), 7.26−7,25 (m, 1H), 6.45 (dd, J = 8.4, 0.8 Hz, 1H), 5.52 (s, 2H), 4.08 (s, 3H), 2.28 (s, 3H) ppm. ^{13}C NMR (151 MHz, $CDCl_3$ δ: 187.8, 166.6, 166.2, 143.2, 142.0, 140.5, 135.0, 134.8, 130.5, 129.5, 128.7, 128.3, 127.1, 125.7, 112.5, 103.9, 67.8, 54.1, 16.5 ppm. IR (ATR): 3063, 2961, 2870, 1671, 1591, 1460, 1330, 1277 cm^{-1}. HRMS ESI-MS-q-TOF for $C_{21}H_{19}NO_3$ [M + Na]$^+$ found, 356.1256 m/z; calcd mass, 356.1263. Mp: 132−133 °C. UPLC−MS (DAD/ESI): t_R = 9.18 min, for $C_{21}H_{19}NO_3$ [M + H]$^+$ found, 334.15 m/z; calcd mass, 334.14.

*[3-(2,3-Dihydro-1,4-benzodioxin-6-yl)-2-methylphenyl]methanol (**5**).* Compound **5** was prepared as described for **3**, using a (3-bromo-2-methylphenyl)methanol (2.0 g, 10.3 mmol), (2,3-dihydrobenzo[*b*]-[1,4]dioxin-6-yl)boronic acid (2.2 g, 12.2 mmol), Pd(dppf)Cl_2·DCM (0.11 g, 0.13 mmol) dissolved in toluene (15.5 mL, and ethanol (5.2 mL). Purification by flash chromatography (0−40% EtOAc in hexane) yielded **5** (2.0 g, 76%) as an off-white solid. ^{1}H NMR (600 MHz, $CDCl_3$) δ: 7.35 (d, J = 7.4 Hz, 1H), 7.21 (t, J = 7.5, 1H), 7.17 (dd, J = 7.5,1.2 Hz, 1H), 6.89 (d, J = 8.3 Hz, 1H), 6.80 (d, J = 2.1 Hz, 1H), 6.75 (dd, J = 8.3, 2.1 Hz, 1H), 4.73 (d, J = 4.8 Hz, 2H), 4.28 (s, 4H), 2.24 (s, 3H) ppm. ^{13}C NMR (151 MHz, $CDCl_3$): 143.1, 142.7, 142.4, 139.3, 135.6, 133.8, 129.7, 126.7, 125.7, 122.7, 118.3, 116.9, 64.5, 64.2, 16.0 ppm. HRMS ESI-MS-q-TOF for $C_{15}H_{14}O_3$ [M + Na]$^+$ 279.0993 m/z; calcd mass, 279.0997. IR (ATR) 3324, 3062, 2980, 2934, 2881, 1507, 1248, 1231 cm^{-1}. Mp: 80.5−81.5 °C. UPLC−MS (DAD/ESI): t_R = 5.92 min, for $C_{15}H_{14}O_3$ [M − OH]$^+$ found, 239.12 m/z; calcd mass, 239.11.

*4-{[3-(2,3-Dihydro-1,4-benzodioxin-6-yl)-2-methylphenyl]-methoxy}-2,5-difluorobenzaldehyde (**6a**).* Compound **6a** was prepared as described for **4a**, using 2,5-difluoro-4-hydroxybenzaldehyde (0.43 g, 2.7 mmol), PPh_3 (0.79 g, 3.0 mmol), **5** (0.70 g, 2.7 mmol) dissolved in THF (21 mL), and solution of DIAD (0.59 mL, 3.0 mmol) in THF (21 mL). Purification by flash chromatography (0−60% EtOAc in hexane) yielded **6a** (0.39 g, 36%) as a colorless solid. ^{1}H NMR (600 MHz, $CDCl_3$) δ: 10.20 (d, J = 2.9 Hz, 1H), 7.59 (dd, $^{3,4}J_{H-F}$ = 10.5, 6.5 Hz, 1H), 7.40−7.37 (m, 1H), 7.25−7.24 (m, 2H), 6.92 (d, J = 8.2 Hz, 1H), 6.85 (dd, $^{3,4}J$ = 11.4, 6.4 Hz, 1H), 6.82 (d, J = 2.0 Hz, 1H), 6.77 (dd, J = 8.3, 2.0 Hz, 1H), 5.21 (s, 2H), 4.31 (s, 4H), 2.27 (s, 3H) ppm. ^{13}C NMR (151 MHz, $CDCl_3$) δ: 185.2 (dd, $^{3,4}J_{C-F}$ = 9.0, 3.0 Hz), 161.9 (d, $^1J_{C-F}$ = 255.6 Hz), 153.6, 153.7, 149.4 (d, $^1J_{C-F}$ = 246.9 Hz), 143.2, 142.9, 142.8, 135.1, 134.6, 133,2, 131.0, 127.9, 125.9, 122.7, 118.4, 118.3, 117.1, 114.2 (dt, $^{2,3}J_{C-F}$ = 20.7, 4.5 Hz), 102.6 (dd, $^{2,3}J_{C-F}$ = 26.0, 4.5 Hz), 71.0, 71.1, 64.6, 16.4 ppm. IR (ATR) 3050, 2924, 1672, 1627, 1508, 1283, 1108, 1063, 985 cm^{-1}. HRMS ESI-MS-q-TOF for $C_{23}H_{18}F_2O_4$ [M + Na]$^+$ 419.1075 m/z; calcd mass, 419.1071. Mp: 160−161 °C. UPLC−MS (DAD/ESI): t_R = 8.45 min, for $C_{23}H_{18}F_2O_4$ [M + H]$^+$ found, 397.09 m/z; calcd mass, 397.12.

*4-{[3-(2,3-Dihydro-1,4-benzodioxin-6-yl)-2-methylphenyl]-methoxy}-2-hydroxy-5-methylbenzaldehyde (**6b**).* Compound **6b** was prepared as described for **4a**, using 2,4-dihydroxy-5-methylbenzaldehyde (0.59 g, 3.9 mmol), PPh_3 (1.01 g, 3.5 mmol), and **5** (0.90 g, 2.7 mmol) dissolved in THF (21 mL) and solution of DIAD (0.74 mL, 3.9 mmol) in THF (21 mL). Purification by flash chromatography (0−60% EtOAc in hexane) yielded **6b** (0.95 g, 69%) as a colorless solid. ^{1}H NMR (600 MHz, $CDCl_3$) δ: 11.45 (s, 1H), 9.70 (s, 1H), 7.42 (dd, J = 6.7, 2.1 Hz, 1H), 7.28−7.23 (m, 4H), 6.92 (d, J = 8.2 Hz, 1H), 6.83 (d, J = 2.1 Hz. 1H), 6.79 (dd, J = 8.2, 2.1 Hz, 1H), 5.13 (s, 2H), 4.31 (s, 4H), 2.25 (s, 3H), 2.21 (s, 3H) ppm. ^{13}C NMR (151 MHz, $CDCl_3$) δ: 194.5, 164.3, 163.3, 143.2, 142.8, 142.6, 135.3, 134.7, 134.5, 134.3, 130.4, 127.3, 125.7, 122.7, 119.7, 118.4, 117.0, 114.6, 99.6, 69.6, 64.6, 16.3, 15.7 ppm. IR (ATR) 2994, 2945, 1635, 1507, 1494, 1304, 1317, 1229, 1131, 1064, 786 cm^{-1}. HRMS ESI-MS-q-TOF for $C_{24}H_{22}O_5$ [M + Na]$^+$ 413.1343 m/z; calcd mass, 413.1365. Mp: 157−158 °C. UPLC−MS (DAD/ESI): t_R = 8.91 min, for $C_{27}H_{27}F_2NO_6$ [M + H]$^+$ found, 391.11 m/z; calcd mass, 391.16.

*5-Chloro-4-{[3-(2,3-dihydro-1,4-benzodioxin-6-yl)-2-methylphenyl]methoxy}-2-hydroxybenzaldehyde (**6c**).* Compound **6c** was prepared as described for **4a**, using solution of 5-chloro-2,4-dihydroxybenzaldehyde (0.67 g, 3.9 mmol), PPh_3 (1.01 g, 3.9 mmol), **5** (0.90 g, 3.5 mmol) in THF (21 mL) and DIAD (0.74 mL, 3.9 mmol) dissolved in THF (21 mL). Purification by flash chromatography (0−60% EtOAc in hexane) yielded **6c** (0.54 g, 37%) as a colorless solid. ^{1}H NMR (600 MHz, $CDCl_3$) δ: 11.43 (s, 1H), 9.70 (s, 1H), 7.55 (s, 1H), 7.45 (dd, J = 6.9, 2.2 Hz, 1H), 7.27−7.24 (m, 2H), 6.91 (d, J = 8.2 Hz, 1H), 6.83 (d, J = 2.1 Hz, 1H),6.77 (dd, J = 8.2, 2.1 Hz, 1H), 6.63 (s, 1H), 5.2 (s, 2H), 4.31 (s, 4H), 2.27 (s, 3H) ppm. ^{13}C NMR (151 MHz, $CDCl_3$) δ: 193.9, 163.1, 161.1, 143.2, 142.8, 142.6, 135.2, 134.2, 133.6, 130.6, 127.4, 125.8, 122.7, 118.4, 117.1, 115.2, 101.7, 70.5, 64.6, 16.4 ppm. IR (ATR) 2954, 2923, 2847, 1646, 1624, 1575, 1493, 1462, 1367, 1243, 1203, 1049, 885, 729 cm^{-1}. HRMS ESI-MS-q-TOF for $C_{23}H_{19}ClO_5$ [M + Na]$^+$ 433.0819 m/z; calcd mass, 433.0819. Mp: 219−220 °C. UPLC−MS (DAD/ESI): t_R = 8.72 min, for $C_{23}H_{19}ClO_5$ [M + H]$^+$ found, 411.11 m/z; calcd mass, 411.10.

*3-(5-{[3-(2,3-Dihydro-1,4-benzodioxin-6-yl)-2-methylphenyl]-methoxy}-2-formyl-4-methylphenoxymethyl)benzonitrile (**7a**).* Cs_2CO_3 (0.25 g, 0,8 mmol), **6b** (0.16 g, 0.8 mmol), 3-(bromomethyl)-benzonitrile (0.15 g, 0.8 mmol) were stirred in DMF (3 mL) at room temperature overnight. The solvent was removed under reduced pressure, and the residue was adsorbed on silica gel 60 and purified by flash chromatography (silica gel, 0−60% EtOAc in hexane). The product was obtained as colorless solid (0.17 g, yield 85%). ^{1}H NMR (600 MHz, DMSO-d_6) δ: 10.26 (s, 1H), 8.02 (s, 1H), 7.87 (d, J = 8.2 Hz, 1H), 7.83 (dt, J = 7.7, 1.4 Hz, 1H), 7.64 (t, J = 7.7 Hz, 1H), 7.53 (d, J = 0.8 Hz, 1H), 7.45 (dd, J = 7.7, 0.8 Hz), 7.26 (t, J = 7.7 Hz, 1H), 7.2 (dd, J = 7.7, 1.2 Hz, 1H), 7.04 (s, 1H), 6.93 (d, J = 8.2 Hz, 1H), 6.80 (d, J = 2.1 Hz, 1H), 6.76 (dd, J = 8.2, 2.1 Hz), 5.40 (s, 2H), 5.28 (s, 2H), 4.28 (s, 4H), 2.23 (s, 3H), 2.13 (s, 3H) ppm. ^{13}C NMR (151 MHz, DMSO-d_6) δ: 187.4, 162.8, 160.9, 143.0, 142.5, 141.7, 138.2, 134.9, 134.4, 134.0, 132.4, 131.9, 129.8, 129.3, 127.6, 125.6, 122.2, 119.4, 118.7, 117.8, 116.8, 111.6, 98.1, 69.1, 69.1, 64.1, 15.9, 15.2 ppm. IR (ATR) 2921, 2229, 1679, 1609, 1580, 1506, 1466, 1273, 1246, 1125, 1052, 783 cm^{-1}. HRMS ESI-MS-q-TOF for $C_{32}H_{27}NO_5$ [M + Na]$^+$ 528.1775 m/z; calcd mass, 528.1787. Mp: 175−176 °C. UPLC−MS (DAD/ESI): t_R = 9.09 min, for $C_{32}H_{27}NO_5$ [M + H]$^+$ found, 506.16 m/z; calcd mass, 506.19.

*3-(4-Chloro-5-{[3-(2,3-dihydro-1,4-benzodioxin-6-yl)-2-methylphenyl]methoxy}-2-formylphenoxymethyl)benzonitrile (**7b**).* Compound **7b** was prepared according to the protocol of **7a**, using Cs_2CO_3 (1.7 g, 5.2 mmol), **6c** (0.54 g, 1.3 mmol), 3-(bromomethyl)-benzonitrile (1.0 g, 5.2 mmol) in DMF (3 mL). Purification by flash chromatography (0−60% EtOAc in hexane) yielded **7b** (0.23 g, yield 33%) as a colorless solid. ^{1}H NMR (600 MHz, $CDCl_3$) δ: 10.37 (s, 1H), 7.91 (s, 1H), 7.72 (s, 1H), 7.69−7.66 (m, 2H), 7.54 (t, J = 7.8 Hz, 1H), 7.40−7.37 (m, 2H), 7.26−7.25 (m, 1H), 6.92 (d, J = 8.2 Hz, 1H), 6.81 (d, J = 2.1 Hz, 1H), 6.77 (dd, J = 8.2, 2.1 Hz, 1H), 6.60 (s, 1H), 5.20 (s, 2H), 5.18 (s, 2H), 4.31 (s, 4H), 2.28 (s, 3H) ppm. ^{13}C NMR (151 MHz, $CDCl_3$) δ: 186.8, 160.7, 160.1, 142.8, 137.3, 135.0,

DOI: 10.1021/acs.jmedchem.7b00293
J. Med. Chem. 2017, 60, 5857−5867

134.4, 133.7, 132.4, 131.5, 130.8, 130.7, 130.4, 130.0, 127.5, 125.9, 122.7, 119.5, 118.4, 118.4, 117.2, 113.3, 98.8, 70.7, 70.0, 64.6, 16.5 ppm. IR (ATR) 3048, 2928, 2850, 2231, 1678, 1596, 1581, 1507, 1409, 1275, 1199, 1067, 1045, 789 cm^{-1}. HRMS ESI-MS-q-TOF for $C_{31}H_{24}ClNO_5$ $[M + Na]^+$ 548.1222 *m/z*; calcd mass, 548.1241. Mp: 151.5−152 °C. UPLC−MS (DAD/ESI): t_R = 9.14 min, for $C_{31}H_{24}ClNO_5$ $[M + H]^+$ found, 525.10 *m/z*; calcd mass, 525.14.

■ ASSOCIATED CONTENT

Supporting Information

The Supporting Information is available free of charge on the ACS Publications website at DOI: 10.1021/acs.jmedchem.7b00293.

Molecular formula strings (CSV)

Details on chemical synthesis of compounds, X-ray data, and NMR data and spectra (PDF)

Accession Codes

Coordinates and structure factors have been deposited in the Protein Data Bank with accession numbers 5N2D (**1a**) and 5N2F (**2a**). Authors will release the atomic coordinates and experimental data upon publication.

■ AUTHOR INFORMATION

Corresponding Author

*E-mail: holak@chemia.uj.edu.pl.

ORCID

Lukasz Skalniak: 0000-0002-6707-6697

Alexander Dömling: 0000-0002-9923-8873

Tad A. Holak: 0000-0001-9369-6024

Author Contributions

K.G. synthesized the compounds and wrote the draft of the manuscript. K.M.Z. performed crystallization of the complexes and solved the structures. P.G. collected X-ray data and refined the structures. K.M., R.T., and L.S. provided support with preparation of expression plasmids and protein purification. B.M. performed and analyzed NMR experiments. G.D., A.D., and T.A.H. analyzed data and wrote the final version of the manuscript. All authors discussed the experiments and commented on the manuscript.

Notes

The authors declare no competing financial interest.

■ ACKNOWLEDGMENTS

This research has been supported in part by a Marie Curie FP7 Reintegration Grant within the 7th European Community Framework Programme and by Grants UMO-2012/06/A/ST5/00224 and UMO-2014/12/W/NZ1/00457 (to T.A.H.) and by the Grants UMO-2011/01/D/NZ1/01169 and UMO-2012/07/E/NZ1/01907 (to G.D.) from the National Science Centre. The research has been carried out with the equipment purchased from the financial support of the European Union structural funds (Grants POIG.02.01.00-12-064/08 and POIG.02.01.00-12-167/08). The research was carried out with the equipment purchased from the financial support of the European Regional Development Fund in the framework of the Polish Innovation Economy Operational Program (Contract POIG.02.01.00-12-023/08). P.G. was supported the National Centre of Science (Grant UMO-2015/19/D/NZ1/02009). K.G. and K.M.Z. have received financial support from the National Science Centre (Grant UMO-2015/19/N/ST5/00347 to K.G. and Grant UMO-2016/20/T/NZ1/00519 to K.M.Z). K.M.Z. has received financial support from the Faculty of Biochemistry, Biophysics and Biotechnology of Jagiellonian University, which is a partner of the Leading National Research Centre (KNOW) supported by the Ministry of Science and Higher Education.

■ ABBREVIATIONS USED

ICB, ommune checkpoint blockage; PD-1, programmed cell death-1; PD-L1, programmed death-ligand-1; PD-L2, programmed death-ligand-2; CTLA-4, cytotoxic T-lymphocyte-associated antigen 4; NSCLC, non-small-cell lung cancer; mAbs, monoclonal antibodies; FDA, U.S. Food and Drug Administration; HTRF, homogeneous time-resolved fluorescence; HAC, high-affinity consensus; GuHCl, guanidine hydrochloride; DIAD, diisopropyl azodicarboxylate; Fab, antigen-binding fragment; K_D, dissociation constant; *t*-Bu XPhos, 2-di-*tert*-butylphosphino-2′,4′,6′-triisopropylbiphenyl; Pd(dppf)Cl_2, [1,1′-Bis(diphenylphosphino)ferrocene]-dichloropalladium(II)

■ REFERENCES

(1) Sharma, P.; Allison, J. P. Immune Checkpoint Targeting in Cancer Therapy: Toward Combination Strategies with Curative Potential. *Cell* **2015**, *161*, 205−214.

(2) Topalian, S. L.; Drake, C. G.; Pardoll, D. M. Immune Checkpoint Blockade: A Common Denominator Approach to Cancer Therapy. *Cancer Cell* **2015**, *27*, 450−461.

(3) Shin, D. S.; Ribas, A. The Evolution of Checkpoint Blockade as a Cancer Therapy: What's Here, What's Next? *Curr. Opin. Immunol.* **2015**, *33*, 23−35.

(4) Hoos, A. Development of Immuno-Oncology Drugs - from CTLA4 to PD1 to the next Generations. *Nat. Rev. Drug Discovery* **2016**, *15*, 235−247.

(5) Khalil, D. N.; Smith, E. L.; Brentjens, R. J.; Wolchok, J. D. The Future of Cancer Treatment: Immunomodulation, CARs and Combination Immunotherapy. *Nat. Rev. Clin. Oncol.* **2016**, *13*, 273−290.

(6) Mahoney, K. M.; Rennert, P. D.; Freeman, G. J. Combination Cancer Immunotherapy and New Immunomodulatory Targets. *Nat. Rev. Drug Discovery* **2015**, *14*, 561−584.

(7) Baumeister, S. H.; Freeman, G. J.; Dranoff, G.; Sharpe, A. H. Coinhibitory Pathways in Immunotherapy for Cancer. *Annu. Rev. Immunol.* **2016**, *34*, 539−573.

(8) Farkona, S.; Diamandis, E. P.; Blasutig, I. M. Cancer Immunotherapy: The Beginning of the End of Cancer? *BMC Med.* **2016**, *14*, 1−18.

(9) Melero, I.; Berman, D. M.; Aznar, M. A.; Korman, A. J.; Gracia, J. L. P.; Haanen, J. Evolving Synergistic Combinations of Targeted Immunotherapies to Combat Cancer. *Nat. Rev. Cancer* **2015**, *15*, 457−472.

(10) Smyth, M. J.; Ngiow, S. F.; Ribas, A.; Teng, M. W. L. Combination Cancer Immunotherapies Tailored to the Tumour Microenvironment. *Nat. Rev. Clin. Oncol.* **2015**, *13*, 143−158.

(11) Wolchok, J. D.; Kluger, H.; Callahan, M. K.; Postow, M. A.; Rizvi, N. A.; Lesokhin, A. M.; Segal, N. H.; Ariyan, C. E.; Gordon, R.-A.; Reed, K.; Burke, M. M.; Caldwell, A.; Kronenberg, S. A.; Agunwamba, B. U.; Zhang, X.; Lowy, I.; Inzunza, H. D.; Feely, W.; Horak, C. E.; Hong, Q.; Korman, A. J.; Wigginton, J. M.; Gupta, A.; Sznol, M. Nivolumab plus Ipilimumab in Advanced Melanoma. *N. Engl. J. Med.* **2013**, *369*, 122−133.

(12) Lazar-Molnar, E.; Yan, Q.; Cao, E.; Ramagopal, U.; Nathenson, S. G.; Almo, S. C. Crystal Structure of the Complex between Programmed Death-1 (PD-1) and Its Ligand PD-L2. *Proc. Natl. Acad. Sci. U. S. A.* **2008**, *105*, 10483−10488.

(13) Lin, D. Y.; Tanaka, Y.; Iwasaki, M.; Gittis, A. G.; Su, H. P.; Mikami, B.; Okazaki, T.; Honjo, T.; Minato, N.; Garboczi, D. N. The PD-1/PD-L1 Complex Resembles the Antigen-binding Fv Domains of

DOI: 10.1021/acs.jmedchem.7b00293
J. Med. Chem. 2017, 60, 5857−5867

Antibodies and T Cell Receptors. *Proc. Natl. Acad. Sci. U. S. A.* **2008**, *105*, 3011−3016.
(14) Zak, K. M.; Kitel, R.; Przetocka, S.; Golik, P.; Guzik, K.; Musielak, B.; Dömling, A.; Dubin, G.; Holak, T. A. Structure of the Complex of Human Programmed Death 1, PD-1, and Its Ligand PD-L1. *Structure* **2015**, *23*, 2341−2348.
(15) Weinmann, H. Cancer Immunotherapy: Selected Targets and Small- Molecule Modulators. *ChemMedChem* **2016**, *11*, 450−466.
(16) Zarganes-Tzitzikas, T.; Konstantinidou, M.; Gao, Y.; Holak, T. A.; Krzemien, D.; Zak, K.; Dubin, G.; Dömling, A. Inhibitors of Programmed Cell Death 1 (PD-1): A Patent Review (2010−2015). *Expert Opin. Ther. Pat.* **2016**, *26*, 973−977.
(17) Zhan, M.-M. M.; Hu, X.-Q. Q.; Liu, X.-X. X.; Ruan, B.-F. F.; Xu, J.; Liao, C. From Monoclonal Antibodies to Small Molecules: The Development of Inhibitors Targeting the PD-1/PD-L1 Pathway. *Drug Discovery Today* **2016**, *21*, 1027−1036.
(18) Chupak, L. S.; Zheng, X. Compounds Useful as Immunomodulators. WO2015034820, March 2015.
(19) Chupak, L. S.; Ding, M.; Martin, S. W.; Zheng, X.; Hewawasam, P.; Connolly, T. P.; Xu, N.; Yeung, K.-S.; Zhu, J.; Langley, D. R.; Tenney, D. J.; Scola, P. M.; Mingo, P. A. Compounds Useful as Immunomodulators. WO2015160641, October 22, 2015.
(20) Zak, K. M.; Grudnik, P.; Guzik, K.; Zieba, B. J.; Musielak, B.; Dömling, A.; Dubin, G.; Holak, T. A. Structural Basis for Small Molecule Targeting of the Programmed Death Ligand 1 (PD-L1). *Oncotarget* **2016**, *7*, 30323−30335.
(21) Catalano, A.; Carocci, A.; Defrenza, I.; Muraglia, M.; Carrieri, A.; Van Bambeke, F.; Rosato, A.; Corbo, F.; Franchini, C. 2-Aminobenzothiazole Derivatives: Search for New Antifungal Agents. *Eur. J. Med. Chem.* **2013**, *64*, 357−364.
(22) Chollet, A.; Mori, G.; Menendez, C.; Rodriguez, F.; Fabing, I.; Pasca, M. R.; Madacki, J.; Korduláková, J.; Constant, P.; Quémard, A.; Bernardes-Génisson, V.; Lherbet, C.; Baltas, M. Design, Synthesis and Evaluation of New GEQ Derivatives as Inhibitors of InhA Enzyme and Mycobacterium Tuberculosis Growth. *Eur. J. Med. Chem.* **2015**, *101*, 218−235.
(23) Shuker, S. B.; Hajduk, P. J.; Meadows, R. P.; Fesik, S. W. Discovering High-Affinity Ligands for Proteins: SAR by NMR. *Science* **1996**, *274*, 1531−1534.
(24) Stoll, R.; Renner, C.; Hansen, S.; Palme, S.; Klein, C.; Belling, A.; Zeslawski, W.; Kamionka, M.; Rehm, T.; Muhlhahn, P.; Schumacher, R.; Hesse, F.; Kaluza, B.; Voelter, W.; Engh, R. A.; Holak, T. A. Chalcone Derivatives Antagonize Interactions between the Human Oncoprotein MDM2 and p53. *Biochemistry* **2001**, *40*, 336−344.
(25) Powers, R. Advances in Nuclear Magnetic Resonance for Drug Discovery. *Expert Opin. Drug Discovery* **2009**, *4*, 1077−1098.
(26) Tan, S.; Chen, D.; Liu, K.; He, M.; Song, H.; Shi, Y.; Liu, J.; Zhang, C. W.-H.; Qi, J.; Yan, J.; Gao, S.; Gao, G. F. Crystal Clear: Visualizing the Intervention Mechanism of the PD-1/PD-L1 Interaction by Two Cancer Therapeutic Monoclonal Antibodies. *Protein Cell* **2016**, *7*, 866−877.
(27) Horita, S.; Nomura, Y.; Sato, Y.; Shimamura, T.; Iwata, S.; Nomura, N. High-Resolution Crystal Structure of the Therapeutic Antibody Pembrolizumab Bound to the Human PD-1. *Sci. Rep.* **2016**, *6*, 1−8.
(28) Lee, J. Y.; Lee, H. T.; Shin, W.; Chae, J.; Choi, J.; Kim, S. H.; Lim, H.; Won Heo, T.; Park, K. Y.; Lee, Y. J.; Ryu, S. E.; Son, J. Y.; Lee, J. U.; Heo, Y.-S. Structural Basis of Checkpoint Blockade by Monoclonal Antibodies in Cancer Immunotherapy. *Nat. Commun.* **2016**, *7*, 13354.
(29) Liu, K.; Tan, S.; Chai, Y.; Chen, D.; Song, H.; Zhang, C. W.-H.; Shi, Y.; Liu, J.; Tan, W.; Lyu, J.; Gao, S.; Yan, J.; Qi, J.; Gao, G. F. Structural Basis of Anti-PD-L1 Monoclonal Antibody Avelumab for Tumor Therapy. *Cell Res.* **2017**, *27*, 151−153.
(30) Na, Z.; Yeo, S. P.; Bharath, S. R.; Bowler, M. W.; Balıkçı, E.; Wang, C.-I.; Song, H. Structural Basis for Blocking PD-1-Mediated Immune Suppression by Therapeutic Antibody Pembrolizumab. *Cell Res.* **2017**, *27*, 147−150.
(31) Maute, R. L.; Gordon, S. R.; Mayer, A. T.; McCracken, M. N.; Natarajan, A.; Ring, N. G.; Kimura, R.; Tsai, J. M.; Manglik, A.; Kruse, A. C.; Gambhir, S. S.; Weissman, I. L.; Ring, A. M. Engineering High-Affinity PD-1 Variants for Optimized Immunotherapy and Immuno-PET Imaging. *Proc. Natl. Acad. Sci. U. S. A.* **2015**, *112*, E6506−6514.
(32) Lazar-Molnar, E.; Scandiuzzi, L.; Basu, I.; Quinn, T.; Sylvestre, E.; Palmieri, E.; Ramagopal, U. A.; Nathenson, S. G.; Guha, C.; Almo, S. C. Structure-Guided Development of a High-Affinity Human Programmed Cell Death-1: Implications for Tumor Immunotherapy. *EBioMedicine* **2017**, *17*, 30−44.
(33) Pascolutti, R.; Sun, X.; Kao, J.; Maute, R. L.; Ring, A. M.; Bowman, G. R.; Kruse, A. C. Structure and Dynamics of PD-L1 and an Ultra-High-Affinity PD-1 Receptor Mutant. *Structure* **2016**, *24*, 1719−1728.
(34) Mueller, U.; Förster, R.; Hellmig, M.; Huschmann, F. U.; Kastner, A.; Malecki, P.; Pühringer, S.; Röwer, M.; Sparta, K.; Steffien, M.; Ühlein, M.; Wilk, P.; Weiss, M. S. The Macromolecular Crystallography Beamlines at BESSY II of the Helmholtz-Zentrum Berlin: Current Status and Perspectives. *Eur. Phys. J. Plus* **2015**, *130*, 141.
(35) Kabsch, W. Integration, Scaling, Space-Group Assignment and Post-Refinement. *Acta Crystallogr., Sect. D: Biol. Crystallogr.* **2010**, *66*, 133−144.
(36) Krug, M.; Weiss, M. S.; Heinemann, U.; Mueller, U. XDSAPP: A Graphical User Interface for the Convenient Processing of Diffraction Data Using XDS. *J. Appl. Crystallogr.* **2012**, *45*, 568−572.
(37) Evans, P. R.; Murshudov, G. N. How Good Are My Data and What Is the Resolution? *Acta Crystallogr., Sect. D: Biol. Crystallogr.* **2013**, *69*, 1204−1214.
(38) McCoy, A. J.; Grosse-Kunstleve, R. W.; Adams, P. D.; Winn, M. D.; Storoni, L. C.; Read, R. J. Phaser Crystallographic Software. *J. Appl. Crystallogr.* **2007**, *40*, 658−674.
(39) Emsley, P.; Lohkamp, B.; Scott, W. G.; Cowtan, K. Features and Development of Coot. *Acta Crystallogr., Sect. D: Biol. Crystallogr.* **2010**, *66*, 486−501.
(40) Adams, P. D.; Afonine, P. V.; Bunkóczi, G.; Chen, V. B.; Davis, I. W.; Echols, N.; Headd, J. J.; Hung, L. W.; Kapral, G. J.; Grosse-Kunstleve, R. W.; McCoy, A. J.; Moriarty, N. W.; Oeffner, R.; Read, R. J.; Richardson, D. C.; Richardson, J. S.; Terwilliger, T. C.; Zwart, P. H. PHENIX: A Comprehensive Python-Based System for Macromolecular Structure Solution. *Acta Crystallogr., Sect. D: Biol. Crystallogr.* **2010**, *66*, 213−221.

DOI: 10.1021/acs.jmedchem.7b00293
J. Med. Chem. 2017, 60, 5857−5867